



Cytoprotective and antioxidant effects of aged garlic extract against adriamycin-induced cardiotoxicity in adult male rats

Ashraf Youssef Nasr^{1,2}, Rasha A. Alshali¹

¹Department of Anatomy, Faculty of Medicine, King Abdulaziz University, Jeddah, Saudi Arabia, ²Department of Anatomy, Faculty of Medicine, Zagazig University, Zagazig, Egypt

Abstract: Adriamycin (ADR) efficacy in cancer chemotherapy is well-established. However, ADR-induced cardiotoxicity remains a significant challenge. Aged garlic extract (AGE) is a natural polyphenol with high antioxidant potential. This study was planned to determine the cytoprotective and antioxidant actions of AGE against the cardiotoxic effect of ADR in rats. Six equal groups, control, ADR-treated (single dose of 10 mg/kg on day 8); AGE-treated (one dose of 250 mg/kg for 14 days); AGE plus ADR-treated (one dose of 250 mg/kg AGE for one week plus ADR injection of 10 mg/kg on day 8); ADR plus AGE-treated (single ADR injection of 10 mg/kg on day 8 plus AGE of 250 mg/kg once from 8th to 14th day); combined AGE plus ADR plus AGE-treated (one dose of 250 mg/kg AGE for 14 days plus single ADR injection of 10 mg/kg on day 8). Sera and cardiac samples were collected on day 15 and prepared for histological, ultrastructural and biochemical study. Disorganization, focal degeneration and necrosis with apoptotic changes of the cardiac myofibrils were observed in ADR-treated rats. Also, reduction in level of total creatine kinase, lactic dehydrogenase, alkaline phosphatase enzymes, glutathione, glutathione-peroxidase, superoxide dismutase, and catalase activities and elevation in malondialdehyde concentration were detected in ADR-treated rats. However, combination of AGE attenuated most of the histopathological, ultrastructural, and biochemical changes induced by ADR. Combination of AGE attenuated the cardiotoxic effects-induced by ADR through its antioxidant and cytoprotective potentials. Therefore, AGE can use as adjunct during administration of ADR in cancer therapy.

Key words: Adriamycin, Aged garlic extract, Heart


Received December 9, 2019; Revised December 27, 2019; Accepted January 4, 2020

Introduction

Adriamycin (ADR), also known as doxorubicin HCl, is a cytotoxic anthracycline antibiotic and efficient antitumor drug for the treatment of variable human solid tumors and leukemias. However, its unfavorable adverse cardiotoxicity

limits its clinical uses [1]. The exact pathogenesis of ADR-induced cardiotoxicity has not been fully elucidated but the most common postulated hypothesis is the formation of free radicals and superoxides that induce nuclear apoptosis, deoxyribonucleic acids (DNA) damage, lipid peroxidation and impairment of the cardiac enzymes [2]. This hypothesis is based on the relative lower content of the cardiac cells to the antioxidant enzymes compared to liver and kidneys. Reduction of these antioxidant enzymes increases the production of excessive free radicals and susceptibility to the oxidative stress that could induce myocardial injury [3]. Moreover, mitochondrial damage, lipid peroxidation, vasoactive amine release, declined activity of Na, K-adenosine triphosphate,

Corresponding author:

Ashraf Youssef Nasr 

Department of Anatomy, Faculty of Medicine, King Abdulaziz University, Jeddah 21589, Saudi Arabia

E-mail: ashrafnaeem2013@gmail.com

Copyright © 2020. Anatomy & Cell Biology

This is an Open Access article distributed under the terms of the Creative Commons Attribution Non-Commercial License (<http://creativecommons.org/licenses/by-nc/4.0/>) which permits unrestricted non-commercial use, distribution, and reproduction in any medium, provided the original work is properly cited.

impaired myocardial adrenergic signaling/regulation and cellular toxicity are supposed to be the other possible mechanisms for the myocardial toxic effects of ADR [2].

The incidence of ADR-induced cardiotoxicity depends on risk factors, genetic predisposition, duration of the therapy, the existence of cardiovascular disorders and combinatory cancer therapy. The results of recent studies revealed that ADR can induce ROS through nicotinamide adenine dinucleotide phosphate oxidase and nitric oxide synthase pathways [4]. Moreover, decreased activity of Na, K-adenosine triphosphate, mitochondrial damage, vasoactive amine release, and cellular toxicity are supposed to be the other possible mechanisms of ADR-induced cardiotoxicity [2]. Different researches proved that ADR-cardiomyopathy is associated with calcium dysregulation, iron metabolism abnormality, DNA damage, endoplasmic reticulum stress, and cell apoptosis [5].

Besides, other various pathways including mitochondrial dysfunction, peroxynitrite formation, autophagy and cardiac inflammation are considered as a complex mechanism that can explain the cardiotoxic effect of ADR [6]. Another theory of ADR-induced cardiotoxicity is the high binding affinity of ADR to the anionic phospholipid cardiolipin within the inner mitochondrial membrane. This mechanism stimulates the cell death program and changes the channeling of the electron transport chain and energy through the separation of cardiolipin-associated proteins from the inner mitochondrial membrane. Binding of cardiolipin with ADR is mediated by oxidative stress and is considered as one mediator of ADR cardiotoxic action [7]. Also, the inhibitory effect of ADR on the number of cardiac progenitor cells and postnatal cardiomyocytes can impair the turnover of cardiomyocytes and increase the number of aged cells [8].

From the previously reported data, ADR-induced cardiotoxicity seems to be a complicated multifactorial pathway. So, different protective strategies are planned to ameliorate the cardiotoxic effect of ADR using variable synthetic and natural products. Two main strategies have been commonly used to reduce ADR cardiotoxicity: structural modification by chemical and pharmaceutical methods and combination by cardioprotective drugs. Therefore, different protective strategies are planned using synthetic and natural products to ameliorate the toxic side effects of ADR without a reduction in their therapeutic efficacy in experimental animal models to approve for clinical use [1, 4]. However, in some experimental studies, the combination of ADR with chemi-

cal antioxidants reveals limited clinical value [6]. So, the growing trends are focused on the herbal extracts, natural products, and traditional medicine preparations that possessed an antioxidant potential to attenuate the cytotoxic effect of the chemotherapeutic agents. Polyphenolic herbals are major nutrients responsible for improving general health and cure various pathological conditions. The natural herbal antioxidants have been used to ameliorate ADR-induced cell damage without compromising its anti-neoplastic efficacy in many experimental animal-model studies [9].

Garlic is one of the most world-wide used traditional medicinal plants for diseases management [10]. Garlic exhibits anticancer, free radical scavenging, immunomodulatory, anti-infection, anti-hypertension, anti-hyperlipidemia, anti-diabetic effects through its high content of the bioactive volatile, non-volatile, and water-soluble organosulfur compounds such as allicin, diallyl sulfide, L-cysteines, alliin, S-allyl cysteines (SAC) and ajoene [11]. The concentrations of these bioactive sulfur compounds differ from raw to the processed garlic forms. Where, the garlic extracts have higher content of water-soluble organosulfur compounds than the fresh garlic and other garlic preparations [10]. The biological activity of the garlic preparations depends mainly on the content of organosulfur compounds. Moreover, the chemical structure and standardization procedures of the garlic preparation determine the antioxidant potency.

Aged garlic extract (AGE) is prepared by immersion the raw garlic slices in low ethanol concentration for 12 months at room temperature. The less irritant and odorless AGE preparation contains a high concentration of S-allyl-mercaptocysteine, SAC, diallyl disulfide and alliin [12]. AGE has higher antioxidant potential due to its higher concentrations of the water-soluble organosulfur compounds compared to other garlic preparations [11]. These organosulfur compounds can scavenge reactive oxygen (ROS) and reactive nitrogen species, increase enzymatic and nonenzymatic antioxidants levels. Through such antioxidant property, AGE can stimulate the antioxidant enzymes; protects lipid, protein, and DNA from oxidation by scavenging ROS; protects cell from oxidative injuries through the increase of glutathione (GSH) content; plays an important role in antineoplastic, anti-inflammatory, and immunomodulation effects [13].

To evaluate whether AGE could attenuate ADR-induced histopathological changes and oxidative stress on the cardiac tissue, this investigation is planned to study the possible protective effects of AGE on ADR-induced cardiotoxicity at

histopathological, ultrastructural and biochemical levels in a rat model.

Aim

This research is carried out to reveal the possible cardio-protective action of AGE on the cardiotoxicity of ADR in adult male albino rats.

Materials and Methods

Animals and study design

Thirty-six adult male Wistar rats, aged 10–12 weeks, were obtained from, King Fahd Research Centre, Jeddah, Saudi Arabia. The animals were housed in plastic cages with 12-hour light and dark cycle, kept under temperature (21°C–24°C), humidity (50%–60%), fed standard diet, and free access to tap water *ad libitum*. The experimental procedures were conducted in accordance with the National Institute of health guide for Care and Use of Laboratory Animals and were approved by the research ethical committee, Faculty of Medicine, King Abdulaziz.

Drugs and chemicals

ADR (Adriablastina, 50 mg vial; Pharmacia Italia SPA, Milan, Italy) was purchased from EIMC United Pharmaceuticals, Egypt. AGE (Kyolic) was purchased from Wakunaga of America (Mission Viejo, CA, USA). Colorimetric kits of creatine phosphokinase (CPK), lactate dehydrogenase (LDH), alkaline phosphatase (ALP), malondialdehyde (MDA) for lipid peroxidation, reduced GSH, glutathione-peroxidase (GSH-Px), catalase (CAT), superoxide dismutase (SOD) enzymes were purchased from Bio-Diagnostic Company, Cairo, Egypt for biochemical assay according to the manufacturer's instructions.

Experimental protocol

Randomly division of the rats was assigned to six groups (6 rats each) after one week of acclimatization as following: (1) control group, (2) AGE-treated group (single oral dose 250 mg/kg of AGE for 14 days [14]), (3) ADR-treated group (a single intraperitoneal (i.p.) injection 10 mg/kg on day 8) [15, 16], (4) AGE plus ADR-treated group (one oral dose 250 mg/kg of AGE for one week plus a single i.p. injection 10 mg/kg of ADR on day 8), (5) ADR plus AGE-treated group (a single i.p. injection 10 mg/kg of ADR on day 8 plus a single oral dose 250 mg/kg of AGE from 8th to 14th day), (6) AGE Plus

ADR plus AGE-treated group (one oral dose 250 mg/kg of for two weeks plus a single i.p. injection 10 mg/kg of ADR on day 8). The rats were observed for lethargy, anorexia, diarrhea, difficulty breathing, bleeding, impaired ambulation, an inability to remain upright, and deaths. Also, the rats were weighed once every other day throughout the experimental period.

Samples collection

At day 15, the animals were weighed and anaesthetized using ether. Blood samples were collected through direct intracardiac injection in non-heparinized labeled test tubes. After 20 minutes, the serum was separated by centrifugation of the blood samples at 4,000 r/min for 15 minutes and stored in a deep freeze at –20°C until used for biochemical assessment. The hearts of the rats were removed, washed with saline, dried with filtered paper, and weighted. The HW/BW ratio was calculated. Part of left ventricle of each heart was sectioned into slices. These slices were divided into two groups; one immediately fixed in 10% buffered formalin for histological studies and the other was fixed in 2.5% glutaraldehyde for ultrastructural examinations. The remaining part of left ventricle of each heart was sliced into small pieces and placed in ice- cold buffer saline for further biochemical analysis.

Histopathologic examination

After 48 hours of 10% buffered formalin-fixation, the cardiac samples were dehydrated through an ascending ethyl alcohol concentrations, cleared in xylol, embedded in paraffin wax blocks, sectioned at 3–5 µm, mounted on glass slides, and stained with haematoxylin and eosin (H&E), Masson's trichrome and periodic acid Schiff's (PAS) [17] and examined by a light microscope.

Ultrastructure examination

The glutaraldehyde-fixed cardiac samples were washed in phosphate buffer three times for 15 minutes each at 4°C, post-fixed in 1% osmium tetroxide solution for 2 hours at 4°C, dehydrated through ascending concentrations of ethyl alcohol, cleared in propylene oxide, embedded in Epon-Araldite mixture (Embed-812; EMS, Fort Washington, PA, USA), and polymerized at 60°C. Semithin sections (1 µm-thick) were cut, stained with 1% toluidine blue, and examined by light microscope to evaluate the histopathological alterations. Ultra-thin sections (50–60 nm thick) were sliced

by ultra-microtome (Leica RM 2125; Leica Biosystems Nussloch, GmbH, Germany), picked up on copper grids, stained with 2% uranyl acetate and lead citrate [18], and examined using a transmission electron microscope (Jeol TEM 1200 EX; Jeol Ltd., Tokyo, Japan) at 80 Kv.

Assessment of serum cardiac enzymes

Serum levels of LDH enzyme [19], ALP enzyme [20], and CPK enzyme [21] activities were estimated spectrophotometry using commercial kits according to the manufacturer's instructions.

Assessment of oxidative stress biomarkers

The sliced ventricular specimens were homogenized in ice-cold KCl (150 mM) and prepared for determination the tissue level of MDA at 532 nm as nmol/g protein [22] for lipid peroxidation, CAT enzyme activity at 240 nm as U/mg protein [23], SOD activity at 480 nm as U/mg protein [24], reduced GSH concentration at 412 nm as mol/g protein [25], and GSH-Px activity at 340 nm for 5 minutes as U/mg tissue [26] using the commercial kits (Biodiagnostic company, Giza, Egypt) according to the manufacturer's instructions.

Statistical analysis

Data were presented as the mean±SD. The one-way ANOVA analysis of variance and Tukey's *post-hoc* multiple comparison tests were performed to examine the difference among the groups. All statistical analyses were made using IBM SPSS Statistics for Windows, Version 22.0 (IBM Co., Armonk, NY, USA). The *P*-value<0.05 was considered statistically significant.

Results

General observation

The rats revealed no mortality in all experimental groups except one rat of ADR-treated group. The remaining ADR-treated animals appeared lethargic, with lusterless scruffy fur, and developed diarrhea.

Body weight, heart weight, and heart weight/body weight ratio

The mean final BW of the control rats recorded a significant difference (*P*<0.05) compared to the other groups. Meanwhile, comparing the final BW of ADR-treated animals, no significant difference was reported with that of the rats treated with AGE before or after ADR injection. Moreover, the HW of control revealed a significant difference (*P*<0.05) compared to that of the other group except AGE-treated group which recorded no significant difference. Meanwhile, the HW of ADR-treated group showed a significant differences (*P*<0.05) compared to the other groups except AGE-pre-treated group. Regarding the ratio between the BW and HW of control group, a significant difference was recorded compared to ADR-treated, AGE-post treated, and combined AGE pre- and post-treated groups (Table 1).

Serum level of the cardiac enzymes

The mean serum level of CPK, ALP, and LDK enzymes' activities of ADR-treated rats reported a significant difference (*P*<0.05) compared to their respective value in control group. However, oral intake of AGE seven days before the injection of ADR, seven days after the injection ADR, or seven days before and seven days after ADR injection, a significant reduction in the activity of serum level of CPK, ALP, and

Table 1. Effect of AGE and/or ADR on BW, HW, HW/BW ratio (gm), and mortality rate (%)

Animal group (number=6 rats)	Initial BW	Pre-ADR BW	Final BW	HW	HW/BW %	Mortality %
Control	204.8±5.9	213.8±5.90	228.0±6.7 ^{a,b,d}	1.33±0.04**	0.59±0.02	0
AGE	198.4±5.6	205.6±4.20	219.2±4.2 ^{a,b,c,d}	1.29±0.30**	0.58±0.03	0
ADR	211.6±4.8	223.4±7.02	201.6±4.2 ^{a,b,c}	0.99±0.13*	0.51±0.06*	16.7
AGE+ADR	211.8±5.5	219.4±5.98	203.0±5.8 ^{a,b,c}	1.10±0.12 *	0.55±0.04	0
ADR+AGE	203.4±6.5	218.2±2.90	206.8±4.7 ^{b,c}	1.14±0.04***	0.48±0.11*	0
AGE+ADR+AGE	209.4±4.3	222.4±5.03	215.0±3.5 ^{a,b,c,d}	1.18±0.09***	0.55±0.04*	0

Values are presented as mean±SD (n=6). AGE, aged garlic extract; ADR, adriamycin; BW, body weight; HW, heart weight; Pre-ADR BW, the BW before injection of ADR. ^aSignificant difference (*P*<0.05) between the final and initial BW of same group; ^bSignificant difference (*P*<0.01) between the BW at the date of ADR-injection and final BW of the same group; ^cSignificant difference (*P*<0.05) from the final BW of the control group; ^dSignificant difference (*P*<0.05) from the final BW of the ADR-treated group. *Significant difference (*P*<0.05) from the HW of control groups. **Significant difference (*P*<0.05) from HW of ADR-treated rats. One-way ANOVA followed by Tukey's *post-hoc* test.

LDH enzymes compared to their respective values in ADR-treated animals. Also, the activity of LDH and CPK enzymes of control rats revealed a significant difference compared to their respective values of the other groups (Table 2).

Tissue oxidant/antioxidant biomarkers

The mean tissue level of MDA, the biomarker of lipid peroxidation, revealed a significant increase in ADR-treated group compared to its respective value in control group. Meanwhile, co-administration of AGE with ADR induced a significant reduction ($P<0.05$) in MDA level compared to its value in ADR-treated animals. Conversely, the injection of ADR produced a significant reduction ($P<0.05$) in the mean tissue level of GSH activity, GSH-Px, CAT, and SOD compared to the control group. Meanwhile, the combination of AGE with ADR resulted in a significant ($P<0.05$) increase in the mean tissue level of GSH, GSH-Px and the activities of tissue SOD and CAT enzymes compared to their respective values in ADR-treated animals. However, the mean tissue levels and activities of these enzymes revealed no significant difference in control group compared to their values in the combined AGE and ADR-treated groups (Table 3).

Table 2. Effect of AGE and/or ADR on serum level of cardiac enzymes

Animal group	CK (U/l)	LDH (U/l)	ALP (U/l)
Control	100.3±7.8 ^b	391.7±61.8 ^b	143.5±8.9 ^b
AGE-treated	100.8±7.4 ^b	395.5±62.2 ^b	144.8±7.7 ^b
ADR-treated	721.7±65.6 ^a	1090±132.8 ^a	49.3±8.6 ^a
AGE pre ADR-treated	421.7±56.4 ^{a,b}	723.3±72.3 ^{a,b}	79.2±7.9 ^{a,b}
AGE post ADR-treatment	375±52.1 ^{a,b}	628.3±83.8 ^{a,b}	91.8±9.9 ^{a,b}
AGE pre- and post ADR-treated	265±53.2 ^{a,b}	536.7±85.0 ^{a,b}	111.5±10.2 ^{a,b}

Values are presented as mean±SD (n=6). AGE, aged garlic extract; ADR, adriamycin; CK, total creatine kinase; LDH, lactic dehydrogenase; ALP, alkaline phosphatase enzymes. ^aSignificant difference ($P<0.05$) vs. control group; ^bSignificant difference ($P<0.05$) vs. ADR-treated group. One-way ANOVA with *post-hoc* Tukey multiple comparison test was used.

Table 3. Effect of AGE and/or ADR on cardiac oxidant and antioxidant tissue enzymes

Animal group (number=6 rats)	MDA (nmol/g)	GSH (μmol/g)	GSH-Px (U/mg)	CAT (U/mg)	SOD (U/mg)
Control	75.7±6.5 ^c	1.20±0.30 ^c	6.6±0.88 ^c	52.7±3.6 ^c	55.8±2.9 ^c
AGE ^a	72.8±7.5 ^c	1.20±0.20 ^c	6.4±0.91 ^c	53.3±2.9 ^c	55.3±3.1 ^c
ADR ^b	111.0±12.7 ^d	0.84±0.15 ^a	3.4±0.73 ^d	37.5±3.5 ^a	43.2±3.8 ^d
AGE+ADR ^c	96.2±8.2 ^{d,e}	0.95±0.16	4.0±0.64 ^d	41.5±3.7 ^a	50±3.2 ^{d,e}
ADR+AGE	93.0±8.8 ^{d,e}	1.00±0.18	4.3±0.86 ^d	44.3±3.4 ^{d,e}	52.8±3.1 ^c
AGE+ADR+AGE	87.8±8.1 ^{d,e}	1.10±0.18 ^c	5.6±0.84 ^c	50.3±3.8 ^c	54.2±2.9 ^c

Values are presented as mean±SD (n=6). AGE, aged garlic extract; ADR, adriamycin; MDA, malondialdehyde; GSH, glutathione; GSH-Px, glutathione-peroxidase; CAT, catalase; SOD, superoxide dismutase. ^aAged garlic extract-treated group; ^bAdriamycin-treated group; ^cThe combined AGE and ADR-treated groups. ^d $P<0.05$ vs. control; ^e $P<0.5$ vs. ADR-treated group. Analyzed by one-way ANOVA followed by Tukey's *post-hoc* test.

Histopathological findings

Normal histological structure of cardiac muscle was observed in both control (Fig. 1A) and AGE-treated (Fig. 1B) groups, where branching cardiac myofibrils (MF) with transverse striations, elongated single and central nuclei, numerous blood capillaries in the connective tissues between the MF were seen in the heart specimens. On the contrary, different areas of cellular degeneration and necrosis, cytoplasmic vacuolization, inflammatory cell infiltration, hemorrhage, and vascular congestion were seen in the specimens of ADR-treated animals (Fig. 1C). Meanwhile, AGE treatment markedly reduced the histopathological changes induced by ADR injection, wherein AGE pre-treated group, small-sized areas of cellular degeneration and necrosis, congested blood vessels (BV) were observed within cardiac tissue (Fig. 1D); in AGE post-treated rats, scattered small areas of cellular degeneration with dilated congested BV and wide intercellular spaces were seen within the histological structure of the cardiac specimens (Fig. 1E); and in combined AGE pre- and post-treated animals, almost normal cardiac myocytes with vascular congestion were reported in cardiac specimens (Fig. 1F).

In Masson trichrome-stained sections, a little amount of collagen fibers was seen between the cardiac MF and around the BV in control (Fig. 2A), AGE-treated (Fig. 2B), and the combined AGE pre- and post-treated (Fig. 2F) groups. However, a relative increase in the amount of collagen fibers was identified around the BV and within the degenerated cardiac areas in ADR-treated animals (Fig. 2C). Conversely, co-administration of AGE with ADR resulted in a remarkable reduction in the amount of collagen fibers between the cardiac MF, within the degenerated cardiac areas, and around the congested BV of AGE pre-treated (Fig. 2D) and AGE post-treated (Fig. 2E) groups.

PAS-stained cardiac sections showed a strong positive reaction within the sarcolemma of cardiac myocytes in con-

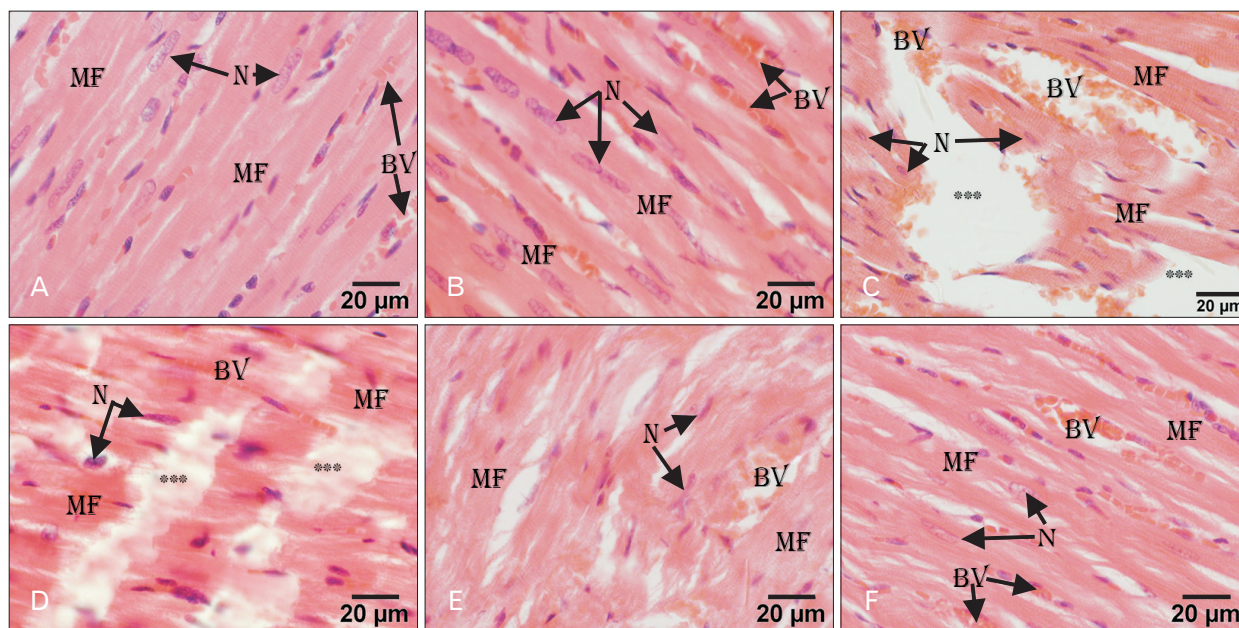


Fig. 1. Light micrographs of rat heart. (A, B) Control and AGE-treated group showing normal organization of the heart structure of branching MF, with myocytes having central elongated N, and numerous BV in-between. (C) ADR-treated showing marked tissue necrosis (***), disorganized degenerated MF, apoptotic N, interstitial edema, and dilated congested BV. (D) AGE pre-treated group showing areas of tissue necrosis (***), degenerated MF, and BV. (E) AGE post-treated group showing minimal myofibrillar degeneration (MF) with the wavy organization and congested BV. (F) Combined pre- and post-AGE treated group showing normally organized MF, myocytes with central elongated N and vascular congestion (BV) in-between. H&E stain, Scale bars=20 µm (A-F). ADR, adriamycin; AGE, aged garlic extract; BV, blood vessels; MF, myofibrils; N, nuclei.

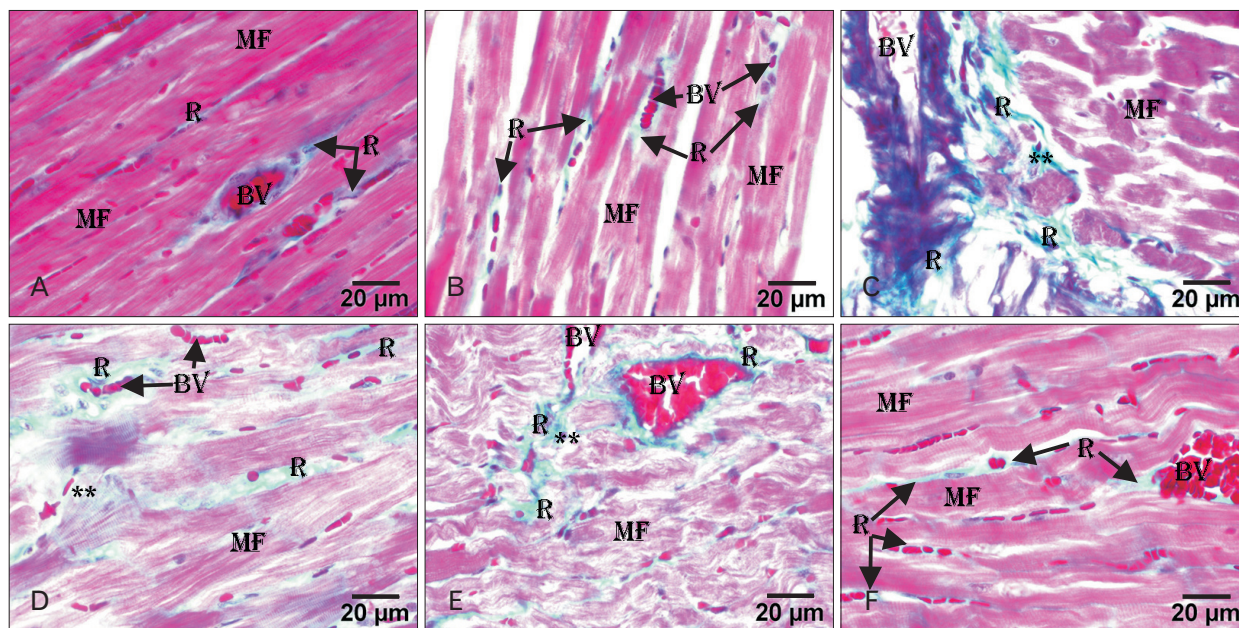


Fig. 2. Light micrographs of rat heart. (A) Control group showing little collagen fibers (R) between the MF and around the BV. (B) AGE-treated group showing minimal collagen fibers (R) between the MF and around the BV. (C) ADR-treated group showing an excessive amount of collagen fibers (R) around the congested BV and between the MF. (D) AGE pre-treated group showing an excessive amount of collagen fibers (R) between the MF and around the BV. (E) AGE post-treated group showing minimal collagen fibers (R) between the cardiac MF and around the BV. (C-E) Symbol ** represent the degenerated area of myocardium. (F) AGE combined pre- and post-treated group showing a minimal amount of collagen fibers (R) between the MF and around the BV. Masson trichrome stain, Scale bars=20 µm (A-F). ADR, adriamycin; AGE, aged garlic extract; BV, blood vessels; MF, myofibrils; R, positive PAS reaction.

trol (Fig. 3A), AGE-treated (Fig. 3B), and combined AGE pre- and post-treated (Fig. 3F) groups. However, the PAS reaction was hardly observed within the cardiac specimen of ADR-treated rats (Fig. 3C). A weak PAS-reaction was seen within the sarcolemma of cardiac MF in AGE pre-treated (Fig. 3D) and AGE post-treated (Fig. 3E) groups.

Electron microscopic findings

By electron microscopic examination, the ultrastructure of the control cardiac tissue showed striated MF with the characteristic sarcomere organization. The sarcomere extended between two neighboring Z-lines. Light filaments in the form of I-band appeared on both sides of Z-line. Dark filaments were in the form of the A-band and H-line. Numerous mitochondria with many transverse cristae and intact limiting membranes appeared as longitudinal columns between the myofilaments. The nucleus of cardiac myocytes appeared regular in shape with a normal distribution of heterochromatin. An abundant amount of mitochondria having

many cristae appeared in the perinuclear space and between the MF (Fig. 4A–C). Scattered regular tubular sarcoplasmic reticulum was seen within the sarcoplasm of the myocytes (Fig. 4A, D). Different junctional complexes appeared between the cardiac myocytes in the form of fascia adherent, macula adherent and gap junction (Fig. 4D).

Moreover, normal cardiac ultrastructure was seen the cardiac tissue of the AGE-treated rats, where well-organized MF were observed with columns of mitochondria in-between (Fig. 5). Regular sarcomeres between the two Z-lines, white filaments around the Z-line, and dark filaments in the form A-bands formed the main structure of the MF. Thin regular sarcolemma formed the outer boundary of the myocytes. Scattered tubular sarcoplasmic reticulum was observed between the MF as well (Fig. 5A–C). The myocytes exhibited a regular elongated central nucleus with multiple small electron-dense nucleoli and scattered heterochromatin masses within the nucleoplasm and on the nuclear envelope inner aspect (Fig. 5B).

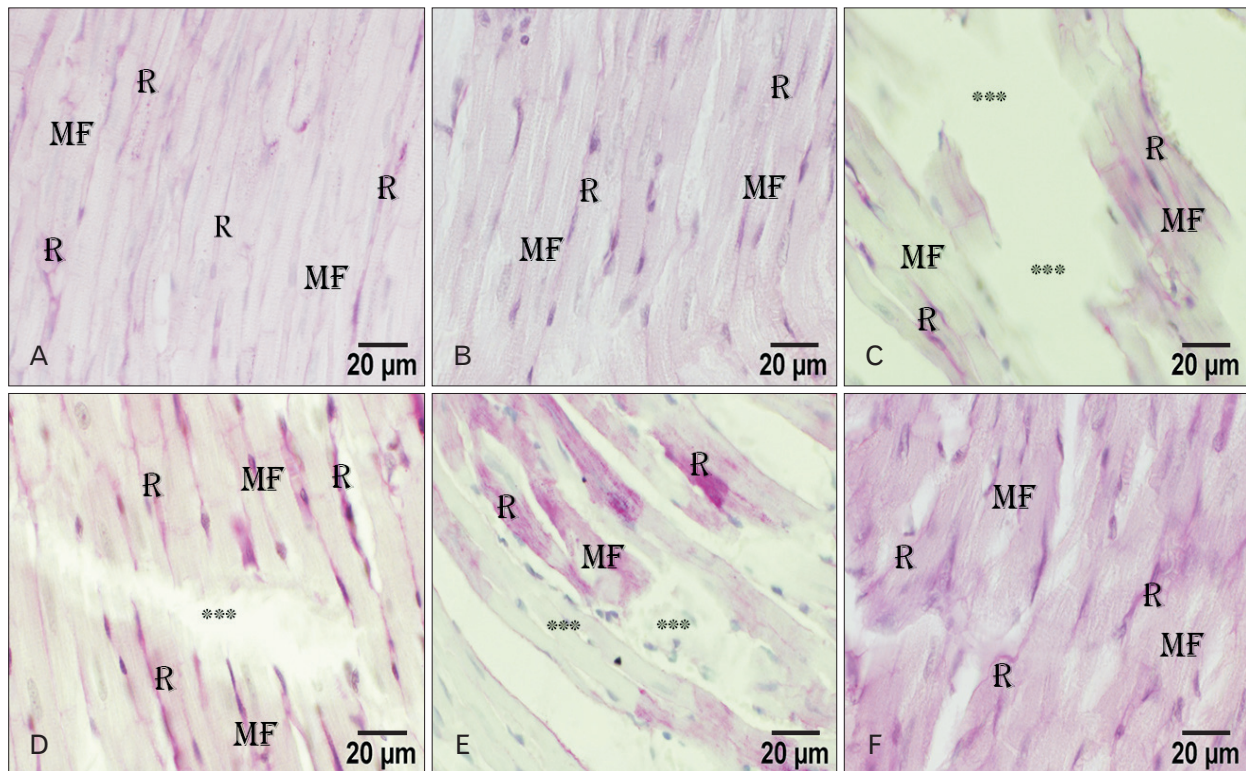


Fig. 3. Light micrographs of the rat heart. (A) Control group showing a R at the perimysium of the MF. (B) AGE-treated group showing a minimal R at the perimysium of the MF. (C) ADR-treated group showing minimal R at the perimysium of the remaining MF. (D) AGE pre-treated group showing a R at the perimysium between the MF. (E) AGE post-treated group showing a R at the perimysium between the MF. (C–E) Symbol *** represent the degenerated area of myocardium. (F) AGE combined pre- and post-treated group showing an excessive R at the perimysium between the MF. PAS stain, Scale bars=20 μm (A–F). ADR, adriamycin; AGE, aged garlic extract; MF, myofibrils; PAS, periodic acid Schiff's; R, positive PAS reaction.

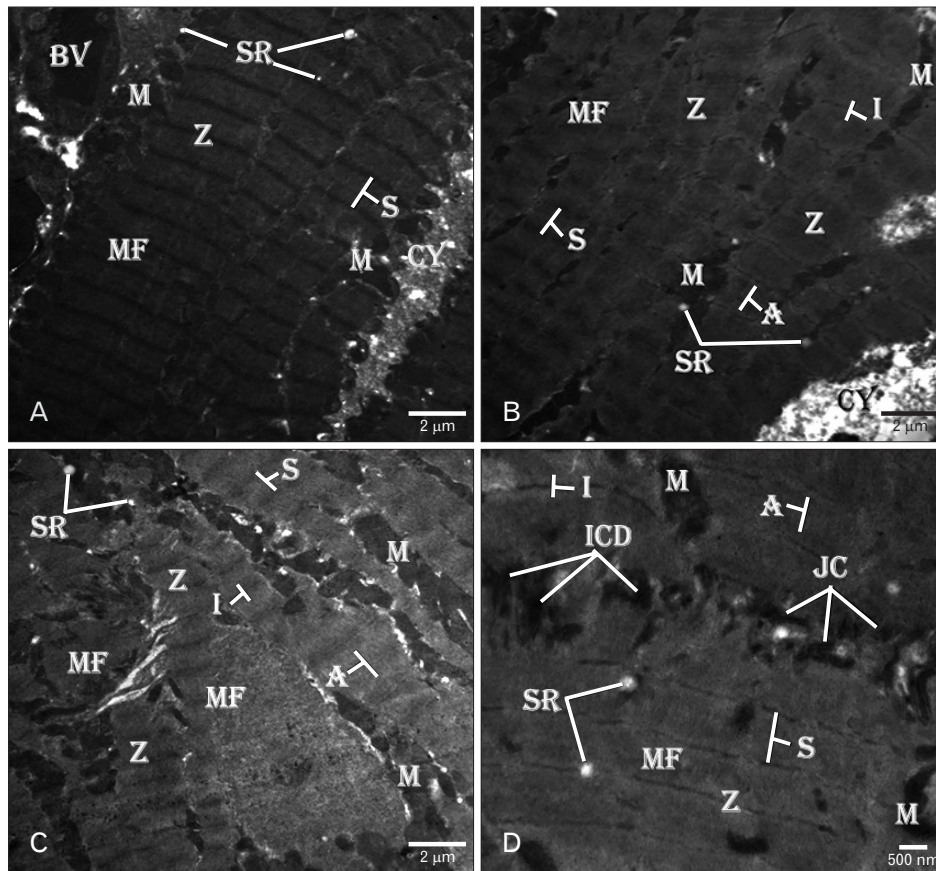


Fig. 4. Electron micrograph of control rat heart showing (A–C) normal organization of branching MF with cross striations. Regular S extends between the two Z. White filament (I-band) surrounds the Z and the dark filaments (A-band) in-between. Columns of M are present between the MF and around the N. Tubular SR is present between the MF near to Z. (D) The ICD is present between two myocytes. The disc consists of different types of JC. TEM osmium tetraoxide-Silver nitrate stains (A–D). Scale bars=2 μ m (A–C), 500 nm (D). BV, blood vessels; CY, cytoplasm; ICD, intercalated disc; JC, junctional complexes; M, mitochondria; MF, myofibrils; N, nucleus; S, sarcomere; SR, sarcoplasmic reticulum; Z, Z-line.

The ultrastructure findings of the ADR-treated cardiac tissue showed disorganized fragmented cardiac MF with marked necrosis, degeneration, and atrophy. Interrupted thick irregular Z-lines were seen with wide intermyofibrillar spaces. No white or dark filaments were recognized within the cardiac tissues. Loose scattered degenerated mitochondria with moth-eating appearance were observed between the MF. The mitochondria exhibited irregular outline, electron-dense condensed matrix, loss of their transverse cristae, and degenerated mitochondrial membranes (Fig. 6A–C). The cardiac myocytes had apoptotic small nuclei with shrinkage nucleoplasm, condensed peripheral heterochromatin, and wide perinuclear space (Fig. 6A). Irregular discontinuous sarcolemmal membrane with wide sub-sarcolemmal space containing heterogeneous matrix formed the outer limits of the cardiac myocytes (Fig. 6A–C). Fragmented, irregular disturbed intercalated discs, that formed the junctional complexes, were seen between the disorganized MF. Short contracted MF were observed around the intercalated disc. Dilated sarcoplasmic reticulum was seen between the MF (Fig. 6D).

The ultrastructure of the rats' hearts treated with AGE for one week before ADR injection (the AGE pre-treated) revealed few disorganized branching MF with apparent white and dark filaments. The MF showed areas of different sizes with degenerative changes. The mitochondria arranged in columns between the MF. Many mitochondria exhibited variable sizes, irregular outline, loss cristae, and condensed matrix. Dilated tubular sarcoplasmic reticulum was seen between the MF (Fig. 7A–C). The myocyte had oblique regular nucleus with the intended nuclear envelope, electron-dense central nucleolus, and numerous scattered masses of the condensed heterochromatin within its nucleoplasm. Few, small-sized mitochondria, electron-lucent vesicles, and electron-dense granules were observed in the wide perinuclear space (Fig. 7B). Less formed intercalated discs with fewer junctional complexes were seen between the myocytes. Few short contracted MF were observed around the intercalated disc (Fig. 7D).

The ultrastructure of the rats' hearts treated with AGE for one week after ADR injection (the AGE post-treated) showed regular branching MF with columns of compact large-sized

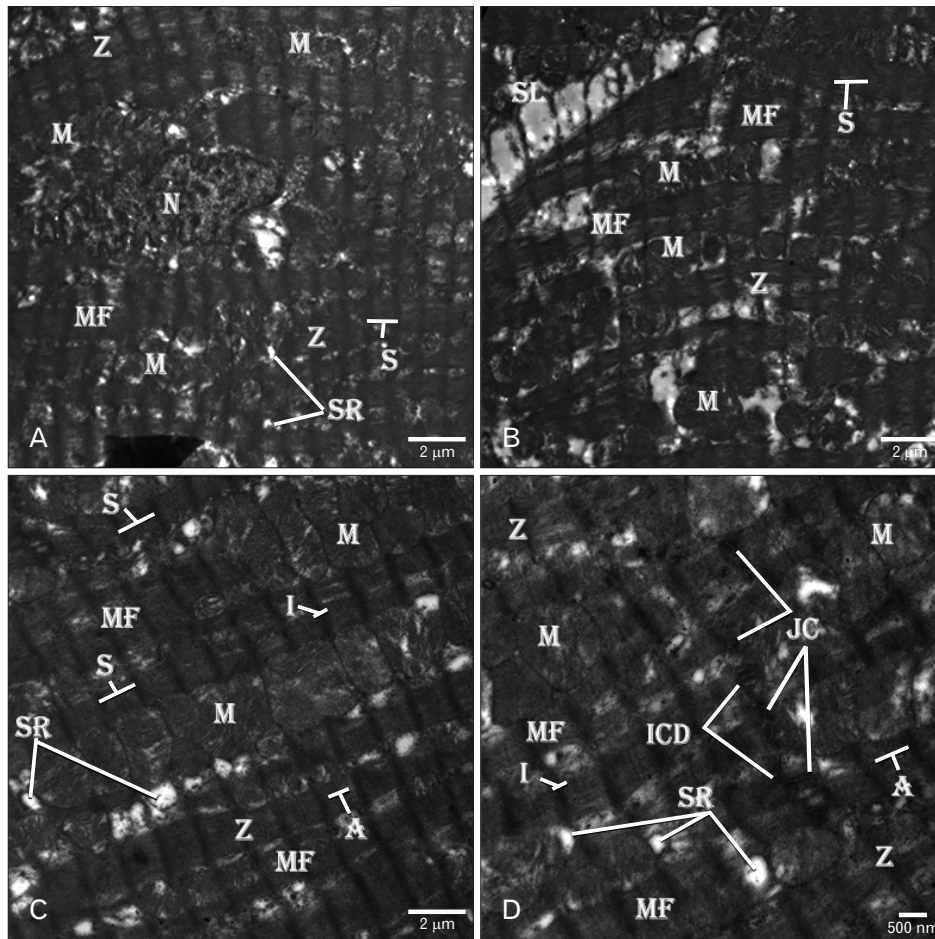


Fig. 5. Electron micrographs of rat heart treated with AGE showing (A–D) normal organization of MF with columns of round M in-between. The MF have cross striations with numerous S between the Z, white filaments (I-band) around the Z and dark filaments (A-band) between the white filaments. The myocyte has a regular SL with subsarcolemmal space (S) underneath. (B) The myocytes have central elongated regular heterochromatic N. Scattered tubular SR is seen between the MF near to the Z. (D) Complex ICD composing of multiple JC are present between the neighboring myocytes. TEM osmium tetraoxide-Silver nitrate stains (A–D). Scale bars=2 μ m (A–C), 500 nm (D). AGE, aged garlic extract; ICD, intercalated disc; JC, junctional complexes; M, mitochondria; MF, myofibrils; N, nucleus; S, sarcomere; SL, sarcolemmal membrane; SR, sarcoplasmic reticulum; Z, Z-line.

normal mitochondria. Regular Z-lines, white and dark filaments were seen within the cardiac tissue. Few degenerated mitochondria were observed between the MF (Fig. 8A–C). The myocytes had a regular sarcolemmal membrane with wide subsarcolemmal space containing electron-dense granules and small mitochondria (Fig. 8B). The myocyte had elongated regular nucleus with many electron-dense nucleoli and heterochromatin masses on the inner aspect of nuclear envelop (Fig. 8B). Complex intercalated disc with different types of junctional complexes was seen between the adjacent myocytes (Fig. 8D).

The ultrastructure of the rats' hearts treated with AGE for one week before and one week after ADR injection (the AGE combined pre- and post-treated) showed the normal structure of regular branching MF with cross striations. The myofibers exhibited well-formed white filaments around the regular Z-lines and dark filaments of A-band and H-band. Columns of large-sized normal mitochondria were seen between the MF. The tubular sarcoplasmic reticulum was

observed between the MF (Fig. 9). The cardiac myocytes had a central elongated nucleus with intended regular nuclear envelop, many electron-dense nucleoli of variable size, granular nucleoplasm, and peripheral electron-dense heterochromatin on the inner aspect of nuclear envelop (Fig. 9B). Complex intercalated discs of different forms of the junctional complexes were observed between the neighboring cardiac myocytes (Fig. 9D).

Discussion

The clinical efficiency of ADR in the treatment of different types of cancers is well-established. However, ADR-induced cardiotoxicity remains a significant challenge [27]. So, different strategies of research and investigation were explored over the years to clarify the exact mechanism of cardiotoxicity induced by ADR [1, 4, 28]. ADR-induced cardiotoxicity seemed to be a multifactorial complicated mechanism, where the oxidative stress, increased lipid per-

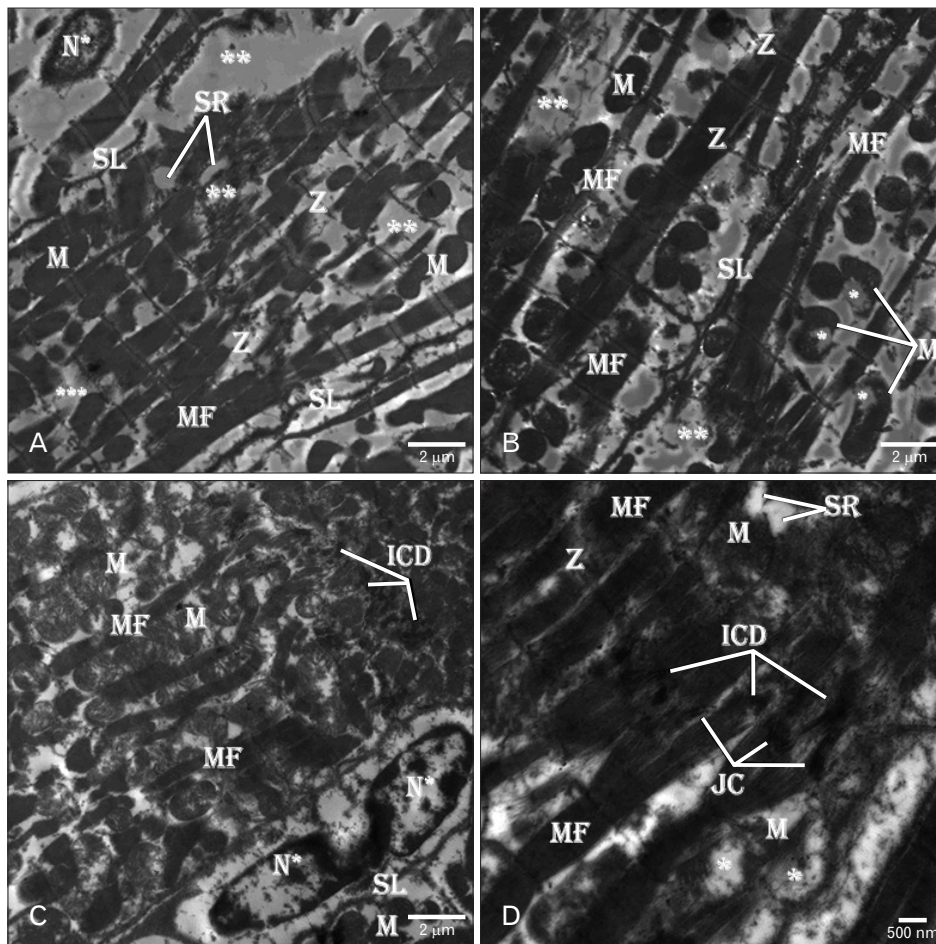


Fig. 6. Electron micrographs of ADR-treated rat heart showing (A–C) marked tissue degeneration and necrosis (**) with MF disorganization. Irregular interrupted Z and SL are seen with cardiac tissue. The myocytes have apoptotic N* with wide electron-lucent perinuclear space. Scattered pleomorphic degenerated M are seen between the atrophic MF. The M show irregular outline, moth-eaten degeneration (*), condensed electron-dense matrix and loss of their cristae. Irregular discontinuing SL is seen limiting the myocytes. (C) Segmented apoptotic N* with peripheral condensed heterochromatin is seen within the myocyte. (C, D) Fragmented ICD composed of loose JC are seen between the myocytes. (D) Short contracted MF and degenerated (*) M are present between the myocytes. TEM osmium tetroxide-Silver nitrate stains (A–D). Scale bars=2 μm (A–C), 500 nm (D). ADR, adriamycin; ICD, intercalated disc; JC, junctional complexes; M, mitochondria; MF, myofibrils; N, nucleus; SL, sarcolemmal membrane; SR, sarcoplasmic reticulum; Z, Z-line.

oxidation, abnormal calcium hemostasis, mitochondrial dysfunction, iron regulatory protein product, nitric oxide release, decrease ATP level, increase inflammatory mediators, endothelial dysregulation, hampered cardiac progenitor cells, autophagy and cell death were implicated in the development of the cardiotoxic mechanism of ADR [1, 4, 27, 29].

Recently, many animals' experimental studies used the natural products and medicinal herbs to attenuate the toxic effect of ADR on the heart [4, 9, 15, 28, 29]. AGE and its components exhibit anti-inflammatory, antihypertensive, anti-hyperlipidemic, anti-diabetic, powerful anti-oxidant and immune modulation effects. So, AGE was used to protect against the toxicity of ADR [15, 30], Acrylamide [31], trichloromethane [32] and cisplatin [14]. The anti-oxidant potential of AGE was mediated through inhibition of lipid peroxidation, increasing glutathione in the cells, and scavenging ROS, enhancing cellular enzymes [10, 12]. So, in the present study, AGE with known anti-oxidant, anti-apoptotic and cytoprotective properties was used to attenuate ADR-

induced morphological, histopathological, ultrastructural, and biochemical cardiotoxic effects in the adult male albino rats [15], where high mortality with a significant reduction of the BW, HW, and HW/BW ratio was recorded 7 days after ADR treatment.

Meanwhile, the co-treatment of ADR-injected animals with oral AGE effectively restored the loss of both body and HWs. The higher mortality in ADR-treated rats might be due to intraperitoneal injection, which could induce serious mucositis with subsequent reduction of food intake, diarrhea, and weight loss [33]. Moreover, the significant reduction of the BWs might be the result of inhibition of protein synthesis and decrease of the food assimilation under effect of ADR on gastrointestinal tract [15, 33, 34], whereas reduction of the HW and HW/BW ratio was the result of the degeneration, necrosis, and atrophy of the cardiac MF under effect of ADR [15, 34]. On the contrary, the combination of oral AGE induced a significant regain of the weight of the body and heart of ADR-injected animals. Such an effect could be in-

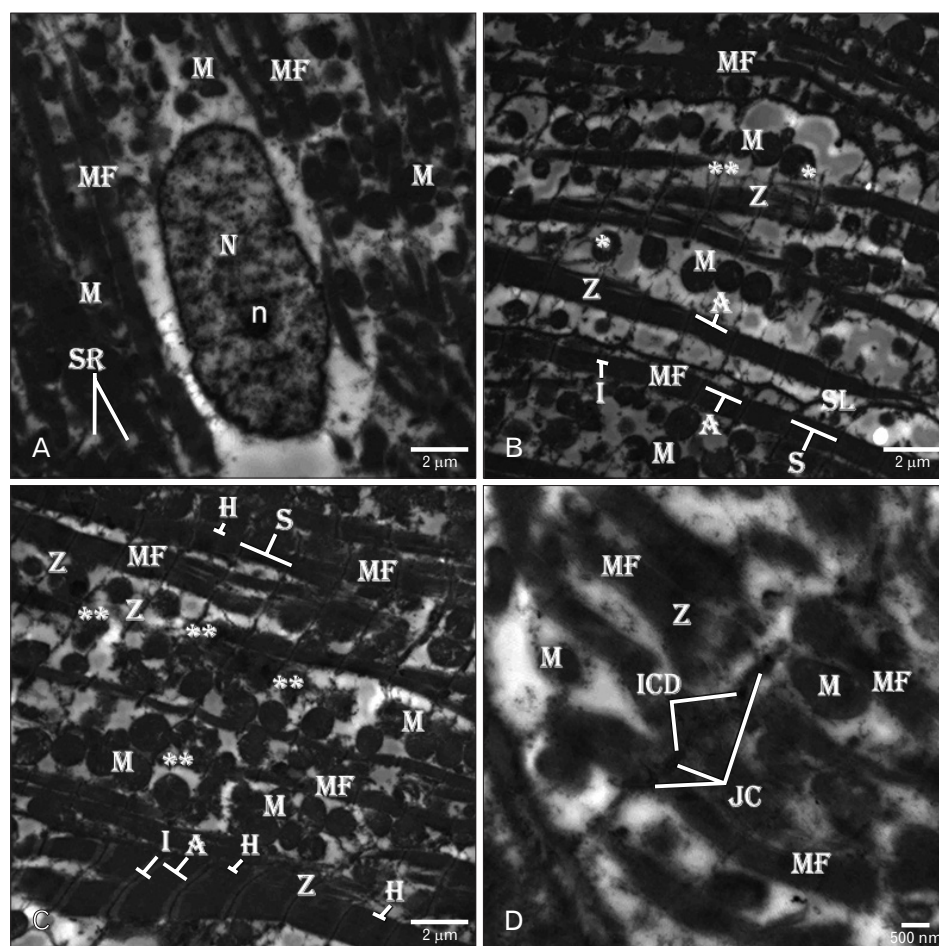


Fig. 7. Electron micrographs of the rats' hearts treated with AGE for one week before ADR injection (AGE pre-treated group) showing (A–C) organized MF with cross striations, well-formed Z, white (I-band) and dark (A-band and H-band) filaments. Symbol * represent the moth-eaten degenerated mitochondria. Scattered area of tissue necrosis (**) is present within the cardiac tissue. Many degenerated M with loss of its cristae are seen between the MF. (A) The myocyte exhibits regular central oblong heterochromatic N with electron-dense n and intended nuclear envelope. (D) An ICD with loose JC is seen between the myocytes. Contracted short myofilaments (MF) are seen around the ICD. TEM osmium tetroxide-Silver nitrate stains (A–D). Scale bars=2 μ m (A–C), 500 nm (D). ADR, adriamycin; AGE, aged garlic extract; ICD, intercalated disc; M, mitochondria; MF, myofibrils; N, nucleus; n, nucleolus; SR, sarcoplasmic reticulum; Z, Z-line.

duced as a result of the improvement of the appetite and food assimilation by AGE. Also, structural regeneration of the cardiac tissue was observed in the combined ADR and AGE-treated groups with significant improvement of the HW. So, AGE seemed to ameliorate the morphological toxic effect of ADR on the weight of both body and heart of the rats in the different experimental groups.

In this study, the morphological changes were supported by the histopathological findings, where structural disorganization, loss striations, myofibrillar degeneration and necrosis, cytoplasmic vacuolization, vascular congestion, and interstitial edema and hemorrhage were seen in the cardiac tissue of ADR-treated animals. In accordance with the findings of this study, similar histopathological changes were previously described by many researchers who supposed that the oxidative stress, lipid peroxidation, and apoptosis were the underlying mechanisms for ADR cardiotoxicity [29, 33, 34]. On contrary, the oral intake of AGE preserved the histological structure and normalizes the architecture of the

cardiac tissue of the ADG-treated animals through its anti-inflammatory, cytoprotective and anti-apoptotic properties [15, 30]. So, AGE exhibited a promising protective effect on ADR-induced cardiotoxicity and could be used as a cytoprotective agent against the toxic effects of different chemotherapeutic drugs in clinical trials.

In the current study, the aforementioned morphological and histopathological changes were further strengthened by the electron microscopic findings, where marked myofibrillar degeneration, cellular disorganization, tissue necrosis, mitochondrial degeneration, nuclear fragmentation and apoptosis, dilated sarcoplasmic reticulum, disturbed intercalated discs, and fragmented sarcolemmal membrane were seen in the cardiac myocytes of ADR-treated rats. Similar findings were reported in ADR-intoxicated rats [16, 34]. The cytoplasmic vacuolization was related to the dilation of sarcoplasmic reticulum [29], while the loss of cardiac MF might be due to the reduction of mRNA expression of troponin I and myosin cardiac-specific proteins [29, 35].

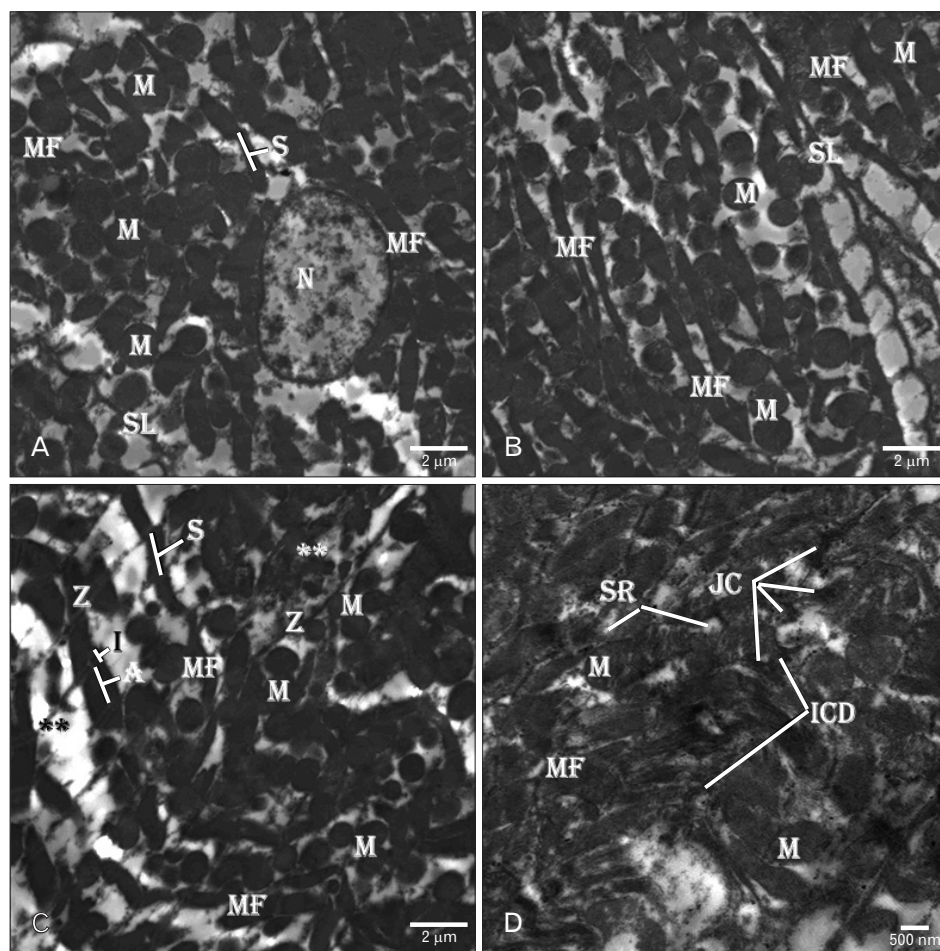


Fig. 8. Electron micrographs of the rats' hearts treated with AGE for one week after ADR injection (AGE post-treated group) showing (A–C) organized branching MF with columns of compact M in-between. The S are present between the regular Z with white filaments (I-band) around and dark filaments (A-band) in-between. H-bands are present at the centre of the dark filaments (A-band). (B) Regular elongated heterochromatic N with wide electron-lucent perinuclear space. Few degenerated M with loss transverse cristae are observed between the MF. (C) Area of myocardium degeneration (**). (D) An ICD consisting of multiple JC is present between the neighboring myocytes. TEM osmium tetroxide-Silver nitrate stains (A–D). Scale bars=2 μm (A–C), 500 nm (D). ADR, adriamycin; AGE, aged garlic extract; ICD, intercalated disc; JC, junctional complexes; M, mitochondria; MF, myofibrils; N, nucleus; S, sarcomere; SL, sarcolemmal membrane; SR, sarcoplasmic reticulum; Z, Z-line.

The dilatation of sarcoplasmic reticulum could increase the openings of Ca^{2+} channels and inhibit $\text{Na}^+ - \text{Ca}^{2+}$ exchanger membrane proteins with subsequent disruption of cell metabolism, excess of free radicals generation, and nuclear apoptosis as a result of cellular and mitochondrial Ca^{2+} overload [29]. However, few studies reported that ADR could induce myocardial hypertrophy and cardiomyopathy with high mortality [36]. Moreover, mitochondrial damage could inhibit fatty acid oxidation; suppress the activity of $\text{N}^+ \text{K}^-$ -ATPase and $\text{Ca}^{2+} - \text{Mg}^{2+}$ ions ATPase enzyme with subsequent reduction of cardiac energy production, and myocardial contraction [33].

The serum level of CPK, LDH, and ALP enzymes is a sensitive indicator on the intactness of the plasma membrane of cardiac cells, as biomarkers of cardiac necrosis, and toxicity. In this study, a marked increase in serum level of CPK, LDH, and ALP enzymes was reported in ADR-treated rats. Such effect might be due to increased lipid peroxidation and sarcolemmal degeneration [28]. In consistent with the find-

ings of this study, ADR induced an obvious elevation in the activities of serum CK, LDH, and CPK enzymes as a result of myocardial injury [34].

The heart protects itself against the oxidative stress through its endogenous antioxidant enzymes. Such enzymes protect the cells against the noxious oxidative stress through detoxification of the superoxide radicals and hydrogen peroxide in cardiac myocytes [37]. So, the heart was considered the main target organ for ADR-induced oxidative stress due to its lower content of endogenous antioxidant enzymes, compared to other organs [29]. Moreover, in the current study, the oxidative damage of ADR in cardiac tissue was evidenced by the significant elevation of lipid peroxidation marker (MDA), reduction of GSH content, decreased activities of CAT, SOD, and GSH-Px enzymes. In this context, the findings of the current study coincided with that of the previous reports [29, 34, 38]. Deficiency of GSH deficiency in ADR-treated animals could be due to its consumption in the interaction of ADR-induced free radicals with bio-mem-

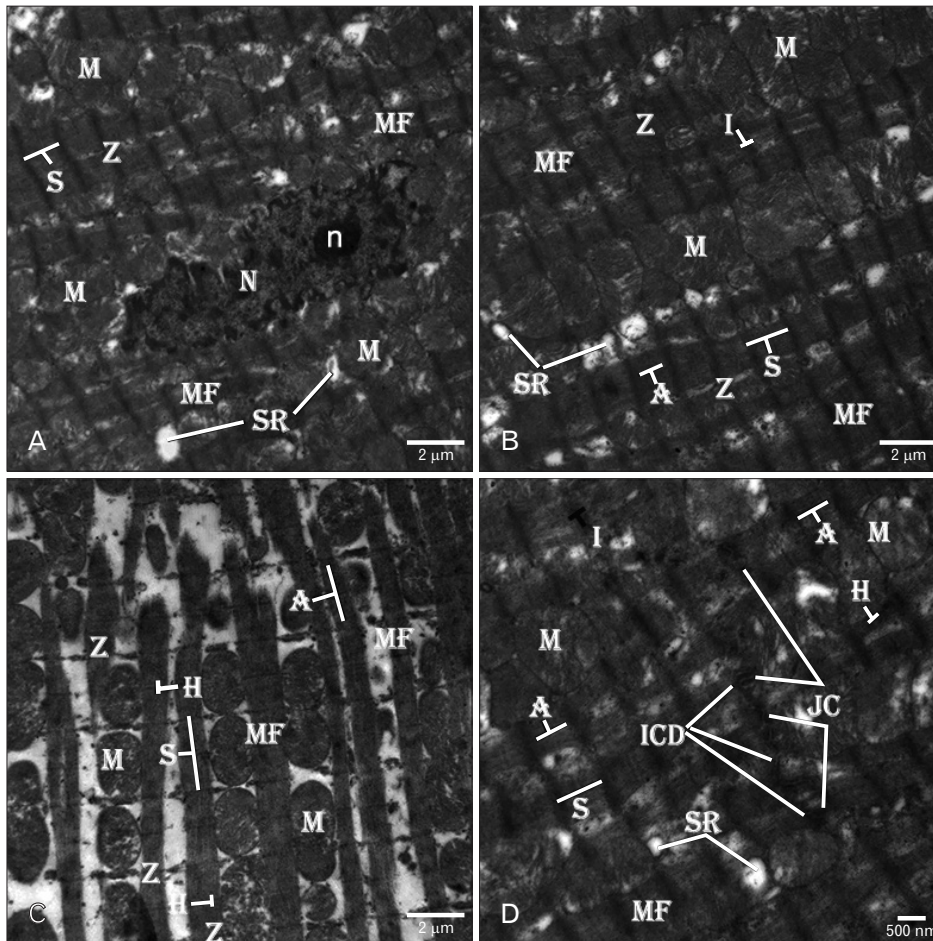


Fig. 9. Electron micrographs of the rats' hearts treated with AGE for one week before and one week after ADR injection (combined AGE pre- and post-treated group) showing (A–D) normal well-organized MF having transverse striations and columns of large-sized regular normal M. The MF have normal white (I-band) and dark (A-band and H-band) filaments. Scattered tubular SR is seen between the MF near to the regular Z. (B) The myocytes have central elongated heterochromatic N with electron-dense small n within its nucleoplasm and an intended regular nuclear envelope. The N is surrounded by groups of rounded-shape normal M and tubular SR. (D) Well-formed ICD with different types of the JC are seen between the adjacent myocytes. The ICD are surrounded by well-organized normal MF with light (I-band) and dark (A-band and H-band) filaments. TEM osmium tetraoxide-Silver nitrate stains (A–D). Scale bars=2 μ m (A–C), 500 nm (D). ADR, adriamycin; AGE, aged garlic extract; ICD, intercalated disc; JC, junctional complexes; M, mitochondria; MF, myofibrils; N, nucleus; n, nucleolus; S, sarcomere; SR, sarcoplasmic reticulum; Z, Z-line.

brane [38]. Furthermore, decrease the activity of antioxidant enzymes in ADR-treated animals might be due to the oxidative stress and high sensitivity of cardiomyocytes to ROS [5, 38].

On the contrary, oral supplementation of AGE to ADR-intoxicated animals effectively restore the imbalance in oxidant/antioxidant enzymes' level in the cardiac tissue. These findings revealed that the cardioprotective effect of AGE against ADR cardiotoxicity through its antioxidant property. In agreement with our results, the previous studies reported the antioxidant potential of AGE through the free radical scavenging properties [15, 30]. The reaction of ADR with iron resulted to an excessive production of free radicals that induced lipid peroxidation with subsequent increase of MDA formation, which representing the breakdown product of lipid peroxidation [39]. In this study, decrease the activity of GSH-Px in DAR intoxicated rats might be due to exhaustion in combating the oxidative stress [40]. Similarly, in this study, oral intake of AGE plus ADR restored the alteration in

the activities of GSH-Px, SOD, and CAT enzymes through the detoxification of ROS induced by ADR and normalization the activity of these enzymes. Also, the remarkable reduction in MDA level as a marker of lipid peroxidation, in the rats treated with AGE plus ADR could be considered as an indication on the antioxidant potential of AGE.

In conclusion, the findings of this study proved that oral co-administration of AGE can attenuate ADR-induced morphological, histopathological, ultrastructural, and biochemical cardiotoxic changes in the adult male rats through its anti-oxidant, anti-inflammatory, and cytoprotective properties. Thus, AGE could be used as an adjuvant therapy with ADR to ameliorate its cardiotoxic effects. In the future, the molecular mechanism of ADR-induced cardiotoxicity, antioxidant and cytoprotective effects of AGE, and the effect of AGE on the therapeutic efficacy of ADR should be investigated to update the strategies controlling ADR-induced cardiotoxicity.

ORCID

Ashraf Youssef Nasr:

<https://orcid.org/0000-0001-7902-669X>

Rasha A. Alshali: <https://orcid.org/0000-0002-4468-1608>

Author Contributions

Conceptualization: AYN. Data acquisition: AYN. Data analysis or interpretation: RAA. Drafting of the manuscript: AYN. Critical revision of the manuscript: AYN. Approval of the final version of the manuscript: all authors.

Conflicts of Interest

No potential conflict of interest relevant to this article was reported.

Acknowledgements

Great appreciations to all technicians of the Electron-microscopic Unit, Faculty of Science, Ain-Shams University for their help during doing this study. This research received no specific grant from any funding agency in the public, commercial or not-for-profit sectors.

References

1. Songbo M, Lang H, Xinyong C, Bin X, Ping Z, Liang S. Oxidative stress injury in doxorubicin-induced cardiotoxicity. *Toxicol Lett* 2019;307:41-8.
2. Renu K, V G A, P B TP, Arunachalam S. Molecular mechanism of doxorubicin-induced cardiomyopathy - an update. *Eur J Pharmacol* 2018;818:241-53.
3. Tham YK, Bernardo BC, Ooi JY, Weeks KL, McMullen JR. Pathophysiology of cardiac hypertrophy and heart failure: signaling pathways and novel therapeutic targets. *Arch Toxicol* 2015;89:1401-38.
4. Yu J, Wang C, Kong Q, Wu X, Lu JJ, Chen X. Recent progress in doxorubicin-induced cardiotoxicity and protective potential of natural products. *Phytomedicine* 2018;40:125-39.
5. Cheung KG, Cole LK, Xiang B, Chen K, Ma X, Myal Y, Hatch GM, Tong Q, Dolinsky VW. Sirtuin-3 (SIRT3) protein attenuates doxorubicin-induced oxidative stress and improves mitochondrial respiration in H9c2 cardiomyocytes. *J Biol Chem* 2015;290:10981-93.
6. Shaker RA, Abboud SH, Assad HC, Hadi N. Enoxaparin attenuates doxorubicin induced cardiotoxicity in rats via interfering with oxidative stress, inflammation and apoptosis. *BMC Pharmacol Toxicol* 2018;19:3.
7. Octavia Y, Kararigas G, de Boer M, Chrifi I, Kietadisorn R, Swinnen M, Duimel H, Verheyen FK, Brandt MM, Fliegner D, Cheng C, Janssens S, Duncker DJ, Moens AL. Folic acid reduces doxorubicin-induced cardiomyopathy by modulating endothelial nitric oxide synthase. *J Cell Mol Med* 2017;21:3277-87.
8. De Angelis A, urbanek K, Cappetta D, Piegari E, Ciuffreda LP, Rivellino A, Russo R, Esposito G, Rossi F, Berrino L. Doxorubicin cardiotoxicity and target cells: a broader perspective. *Cardio-Oncology* 2016;2:2.
9. Lam W, Jiang Z, Guan F, Huang X, Hu R, Wang J, Bussom S, Liu SH, Zhao H, Yen Y, Cheng YC. PHY906(KD018), an adjuvant based on a 1800-year-old Chinese medicine, enhanced the anti-tumor activity of Sorafenib by changing the tumor microenvironment. *Sci Rep* 2015;5:9384.
10. Moutia M, Habti N, Badou A. In vitro and *in vivo* immunomodulator activities of allium sativum L. *Evid Based Complementary Altern Med* 2018;2018:4984659.
11. Arreola R, Quintero-Fabián S, López-Roa RI, Flores-Gutiérrez EO, Reyes-Grajeda JP, Carrera-Quintanar L, Ortuño-Sahagún D. Immunomodulation and anti-inflammatory effects of garlic compounds. *J Immunol Res* 2015;2015:401630.
12. Wang X, Zhang M, Yang Y. The vivo antioxidant activity of self-made aged garlic extract on the d-galactose-induced mice and its mechanism research via gene chip analysis. *RSC Adv* 2019;9:3669-78.
13. Jeong YY, Ryu JH, Shin JH, Kang MJ, Kang JR, Han J, Kang D. Comparison of anti-oxidant and anti-inflammatory effects between fresh and aged black garlic extracts. *Molecules* 2016;21:430.
14. Nasr AY, Saleh HA. Aged garlic extract protects against oxidative stress and renal changes in cisplatin-treated adult male rats. *Cancer Cell Int* 2014;14:92.
15. Nasr AY. The impact of aged garlic extract on adriamycin-induced testicular changes in adult male Wistar rats. *Acta Histochem* 2017;119:648-62.
16. Zhang J, Cui L, Han X, Zhang Y, Zhang X, Chu X, Zhang F, Zhang Y, Chu L. Protective effects of tannic acid on acute doxorubicin-induced cardiotoxicity: Involvement of suppression in oxidative stress, inflammation, and apoptosis. *Biomed Pharmacother* 2017;93:1253-60.
17. Bancroft JD, Layton C. The hematoxylin and eosin. In: Bancroft JD, Layton C, Suvarna KS, editors. *Theory and practice of histological techniques*. 7th ed. Philadelphia: Elsevier, 2012. p. 172-214.
18. Hayat MA. Chemical Fixation. In: Hayat MA, editor. *Principles and techniques of electron microscopy: biological applications*. 4th ed. Cambridge: Cambridge University Press, 2000. p. 4-85.
19. Buhl SN, Jackson KY. Optimal conditions and comparison of lactate dehydrogenase catalysis of the lactate-to-pyruvate and pyruvate-to-lactate reactions in human serum at 25, 30, and 37 degrees C. *Clin Chem* 1978;24:828-31.
20. Tietz NW, Rinker AD, Shaw LM. International Federation of

- Clinical Chemistry. IFCC methods for the measurement of catalytic concentration of enzymes. Part 5. IFCC method for alkaline phosphatase (orthophosphoric-monoester phosphohydrolase, alkaline optimum, EC 3.1.3.1). IFCC document stage 2, draft 1, 1983-03 with a view to an IFCC recommendation. Clin Chim Acta 1983;135:339F-67F.
21. Hørdler M, Elser RC, Gerhardt W, Mathieu M, Sampson EJ. International Federation of Clinical Chemistry (IFCC): scientific division, committee on enzymes. IFCC methods for the measurement of catalytic concentration of enzymes. Part 7. IFCC method for creatine kinase (ATP: creatine (N-phosphotransferase, EC 2.7.3.2). IFCC recommendation. J Automat Chem 1990; 12:22-40.
 22. Ohkawa H, Ohishi N, Yagi K. Assay for lipid peroxides in animal tissues by thiobarbituric acid reaction. Anal Biochem 1979; 95:351-8.
 23. Aebi H. Catalase *in vitro*. Methods Enzymol 1984;105:121-6.
 24. Sun Y, Oberley LW, Li Y. A simple method for clinical assay of superoxide dismutase. Clin Chem 1988;34:497-500.
 25. ELLMAN GL. Tissue sulfhydryl groups. Arch Biochem Biophys 1959;82:70-7.
 26. Lawrence RA, Burk RF. Glutathione peroxidase activity in selenium-deficient rat liver. Biochem Biophys Res Commun 1976; 71:952-8.
 27. Damiani RM, Moura DJ, Viau CM, Caceres RA, Henriques JAP, Saffi J. Pathways of cardiac toxicity: comparison between chemotherapeutic drugs doxorubicin and mitoxantrone. Arch Toxicol 2016;90:2063-76.
 28. Chen X, Peng X, Luo Y, You J, Yin D, Xu Q, He H, He M. Quercetin protects cardiomyocytes against doxorubicin-induced toxicity by suppressing oxidative stress and improving mitochondrial function via 14-3-3 γ . Toxicol Mech Methods 2019;29: 344-54.
 29. Abdel-Daim MM, Kilany OE, Khalifa HA, Ahmed AAM. Allicin ameliorates doxorubicin-induced cardiotoxicity in rats via suppression of oxidative stress, inflammation and apoptosis. Cancer Chemother Pharmacol 2017;80:745-53.
 30. Alkreathy HM, Damanhoury ZA, Ahmed N, Slevin M, Osman AM. Mechanisms of cardioprotective effect of aged garlic extract against doxorubicin-induced cardiotoxicity. Integr Cancer Ther 2012;11:364-70.
 31. Abd El-Halim SS, Mohamed MM. Garlic powder attenuates acrylamide-induced oxidative damage in multiple organs in rat. J Appl Sci Res 2012;8:168-73.
 32. Somade OT, Adedokun AH, Adeleke IK, Taiwo MA, Oyeniran MO. Diallyl disulfide, a garlic-rich compound ameliorates trichloromethane-induced renal oxidative stress, NFkB activation and apoptosis in rats. Clin Nutr Exp 2019;23:44-59.
 33. Wu R, Wang HL, Yu HL, Cui XH, Xu MT, Xu X, Gao JP. Doxorubicin toxicity changes myocardial energy metabolism in rats. Chem Biol Interact 2016;244:149-58.
 34. Mantawy EM, Esmat A, El-Bakly WM, Salah ElDin RA, El-Deimerdash E. Mechanistic clues to the protective effect of chrysin against doxorubicin-induced cardiomyopathy: Plausible roles of p53, MAPK and AKT pathways. Sci Rep 2017;7:4795.
 35. Takemura G, Fujiwara H. Doxorubicin-induced cardiomyopathy from the cardiotoxic mechanisms to management. Prog Cardiovasc Dis 2007;49:330-52.
 36. Lončar-Turukalo T, Vasić M, Tasić T, Mijatović G, Glumac S, Bajić D, Japunžić-Žigon N. Heart rate dynamics in doxorubicin-induced cardiomyopathy. Physiol Meas 2015;36:727-39.
 37. Pisoschi AM, Pop A. The role of antioxidants in the chemistry of oxidative stress: A review. Eur J Med Chem 2015;97:55-74.
 38. Zhang QL, Yang JJ, Zhang HS. Carvedilol (CAR) combined with carnolic acid (CAA) attenuates doxorubicin-induced cardiotoxicity by suppressing excessive oxidative stress, inflammation, apoptosis and autophagy. Biomed Pharmacother 2019; 109:71-83.
 39. Halliwell B, Gutteridge J. Free radicals in biology and medicine. 4th ed. Oxford: Oxford University Press, 2007.
 40. Elberry AA, Abdel-Naim AB, Abdel-Sattar EA, Nagy AA, Mosli HA, Mohamadin AM, Ashour OM. Cranberry (Vaccinium macrocarpon) protects against doxorubicin-induced cardiotoxicity in rats. Food Chem Toxicol 2010;48:1178-84.